Science Advances
AAAS

advances.sciencemag.org/cgi/content/full/7/17/eabf3503/DC1

Supplementary Materials for

Groundwater residence time estimates obscured by anthropogenic carbonate

Alan M. Seltzer*, David V. Bekaert, Peter H. Barry, Kathryn E. Durkin, Emily K. Mace, Craig E. Aalseth, Jake C. Zappala, Peter Mueller, Bryant Jurgens, Justin T. Kulongoski

*Corresponding author. Email: aseltzer@whoi.edu

Published 21 April 2021, *Sci. Adv.* **7**, eabf3503 (2021)
DOI: 10.1126/sciadv.abf3503

The PDF file includes:

Other Supplementary Material for this manuscript includes the following:

(available at advances.sciencemag.org/cgi/content/full/7/17/eabf3503/DC1)

SUPPLEMENTARY INFORMATION

Appendix S1: Modeling residence time distributions, tracer activities, and groundwater mixing

In this study, 17 wells were sampled at least once for ^{3}H and ^{14}C analyses and six wells were targeted for a multiple age-tracer analysis. A map of the study area and depth-distance cross-section showing the screened depth intervals and relative positions of each well is shown in Supplementary Figures S1 and S2. Each of these six wells was sampled for measurement of at least three of the following five tracers: ^{39}Ar (269-yr half-life), ^{14}C (5730-yr half-life), ^{3}H (12.32-yr half-life), ^{85}Kr (10.76-yr half-life) and ^{81}Kr (229-kyr half-life). The purpose of this analysis to investigate consistency between traditional (^{14}C, ^{3}H) and novel (^{39}Ar, ^{81}Kr, ^{85}Kr) age tracers and to better constrain the residence time distributions of groundwater in an important agricultural region. Table S1 provides the measured ^{85}Kr, ^{39}Ar, ^{14}C, ^{3}H, ^{81}Kr, pH, and $\delta^{13}C$ values associated with these case-study wells.

Table S1: Age tracer measurements and well information. Interval refers to the perforated depth interval of well (meters below land surface). Total analytical uncertainties (±2σ), including sampling, storage, and measurement, are estimated to be ±5 pmAr (^{39}Ar), ±5 pmC (^{14}C), ±5 pmKr (^{81}Kr), ±0.1 TU (^{3}H), ±10% of value (^{85}Kr), and ±0.5‰ ($\delta^{13}C$). Mean values are provided for those wells analyzed multiple times. (BL = below detection limit). *n* refers to mixing parameter for partial-exponential mixing model (described below, equation S4).

Well Identification				**^{85}Kr**	**^{39}Ar**	**^{14}C**	**^{3}H**	**^{81}Kr**	**pH**	***n***	**Interval**
USGS Station ID	*GAMA ID*	*NAWQA ID (CVAL-)*	*Alt ID*	*dpm/cc*	*pmAr*	pmC	*TU*	*pmKr*			*m*
364200119420001	KINGFP-02	ETN1-01	180-1	0.44	22.6	48.5	0.0	110	8.0	2.92	125-186
364200119420002		ETN1-02	180-2	9.53		108.1	1.6	101	7.4	1.89	49-95
364200119420003		ETN1-03	180-3	3.8		110.2	1.1	100	7.4	19.80	65-68
364200119420004		ETN1-04	180-4	0.75		39.5	0.1	99	8.2	29.10	179-185
364156119475201	KING-17	PAS1-18	170		23.4	69.0	0.1		7.8	1.92	98-195
364239119440901	KINGFP-03	ETN1-183	183		50.2	42.8	0.0		8.1	5.41	136-165

List of Wells at Each Site:

a: 364156119470001 364156119475201 (170)	**c:** 364239119440901 (183)	**e:** 364418119415101	**g:** 364255119372501 364255119372502 364255119372503	**h:** 364338119354601 364338119354602 364338119354603
b: 364315119451801	**d:** 364200119420001 (180-1) 364200119420002 (180-2) 364200119420003 (180-3) 364200119420004 (180-4)	**f:** 364259119385402 364259119385403		

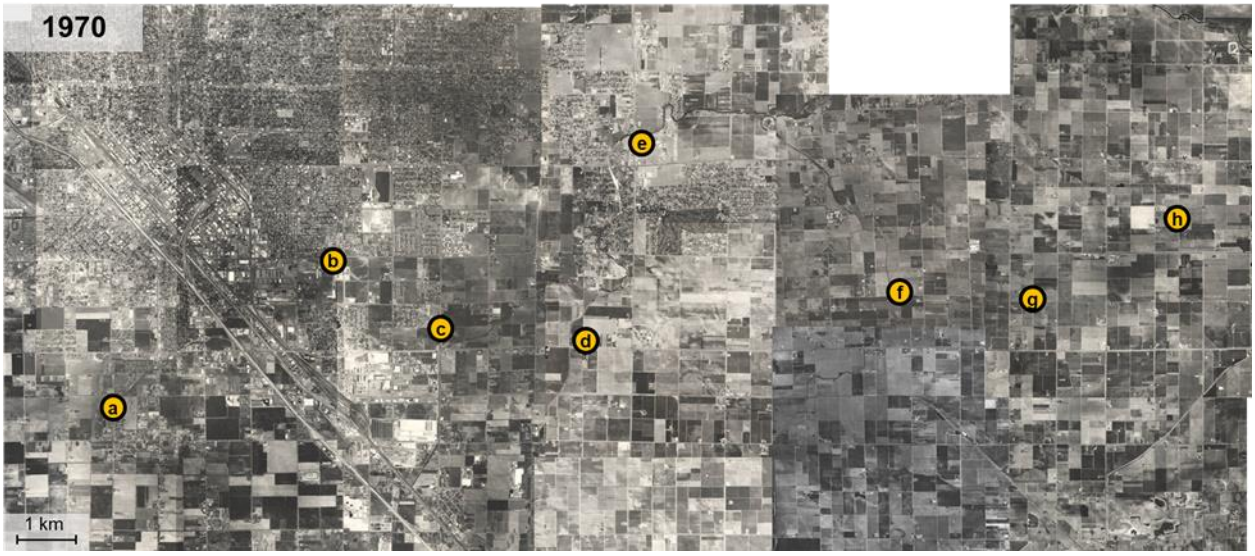

Figure S1. Aerial imagery of study area from 2019 and 1970. **(a-top)** 2019 satellite imagery (from Google Earth) of main study area showing location of eight well clusters (17 wells in total, indicated by USGS Stadion IDs and Alt IDs [see Table S1]), **(b-bottom)** 1970 aerial photographs of study area stitched to produce composite image for comparison of land cultivation surrounding well clusters in main study area. Photographs available from Fresno State University database (http://malt.library.fresnostate.edu/MALT/).

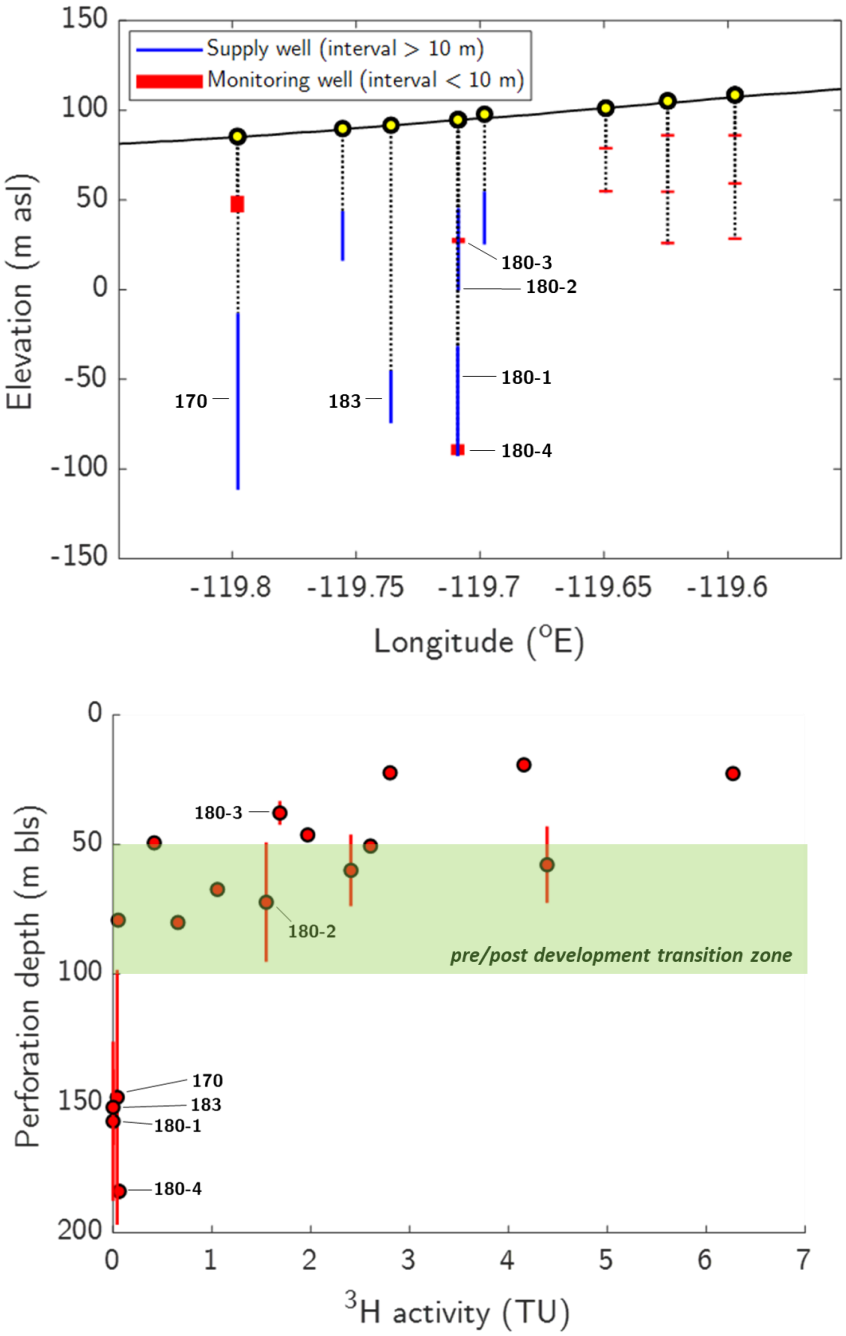

Figure S2: Depths, locations, and tritium content of wells in this study. **(a-top)** Perforated depth intervals of all wells. Yellow circles indicate surface location of single wells or well clusters. Case study wells identified by Alt-IDs (see Table S1); **(b-bottom)** Screened depth intervals for all wells in this study versus mean ^{3}H activity. Wells screened between 50 and 100 m may straddle the interface between the pre-development and post-development groundwater regimes. Wells considered in the multiple age-tracer case study are identified with labels.

The inclusion of radioactive tracers with order 10-yr, order 100-yr, and order 1000-yr half-lives provides a unique opportunity to investigate the applicability of physical mixing models as well as identify systematic offsets between inert and chemically active tracers. We employ lumped-parameter models (LPMs) to explore the age-tracer constraints from these three deep wells, which fall below the transitional depth region between modern and pre-development groundwater regimes (Figure S2b). The theoretical basis for the LPM technique is that the current activity of each radioactive tracer (A) in groundwater is the product of its initial activity (A_0) and radioactive decay integrated across a distribution of individual residence times ($g(t)$) for all parcels comprising a groundwater sample:

$$A = \int_0^\infty A_0 e^{-\lambda t} g(t) dt \qquad \text{(S1)}$$

Our discussion below follows the formulation of two LPMS (one that accounts for mixing and one that does not) outlined in TracerLPM (*45*). These LPMs depend on the mean groundwater residence time τ, which is simply defined:

$$\tau = \int_0^\infty g(t) dt \qquad \text{(S2)}$$

The simplest conceptual LPM is the piston-flow (PF) model, which assumes that groundwater flows from its recharge site to its sampling site without dispersive mixing. The piston-flow model residence time distribution is a dirac delta function:

$$g(t) = 1 \text{ for } t = \tau;\ g(t) = 0 \text{ for } t \neq \tau \text{ (S3)}$$

where τ is the mean groundwater residence time in years.

By convolving $g(t)$ with radioactive decay (equation S1), tracer concentrations are simulated as a function of τ. Although the piston-flow model is the least physically realistic for wells with long screened intervals in an unconfined aquifer, it serves as a useful conceptual starting point. For example, consider the three deep (100-200 m) wells for which ^{14}C and ^{39}Ar were both measured (wells 180-1, 170, 183). In these wells, ^{39}Ar varies between 22.6 and 50.2 percent modern argon (pmAr) and ^{14}C varies between 42.8 and 69.0 pmC. Clearly, to observe both ^{14}C and ^{39}Ar activities near one half the (pre-1950s) atmospheric value requires (a) mixing between young and old waters, and/or (b) an initial ^{14}C activity ($^{14}C_0$) below that of the atmosphere at the time of recharge. Considering a simple binary mixture two groundwater parcels with different mean piston-flow ages, τ, it is clear that the older endmember would have to be nearly ^{14}C free (and thus tens of thousands of years old) and the younger endmember would have to be decades old (sufficiently old to be free of ^{3}H and ^{85}Kr) to yield roughly 50 pmC and 50 pmAr ^{14}C and ^{39}Ar activities. However, the warm (>20 ºC) noble gas-derived recharge temperatures (Supplementary Data Set) temperatures and >99 percent modern krypton (pmKr) ^{81}Kr activities observed in deep wells deep (100-200 m) provide strong evidence against any substantial mixing contribution from pre-Holocene groundwater (older than ~12000 years). Thus, despite its simplicity, the piston flow model provides a useful qualitative indication that mixing alone is insufficient to explain the low ^{14}C activities observed in deep wells. This implies an important role for departures of $^{14}C_0$ from $^{14}C_{atm}$ at the time of recharge. Our primary goals in this case study are therefore to simultaneously estimate $g(t)$ and Γ (where $^{14}C_0 = \Gamma {}^{14}C_{atm}$) using observed age tracer measurements as constraints.

The most physically realistic LPM for the deeper wells in this study is the partial-exponential mixing (PEM) model. The PEM model is applicable for a homogenous unconfined aquifer with a uniform recharge rate, such that the mean age of groundwater decreases exponentially with depth (*44*), but where only a subset of the full aquifer thickness is sampled over the perforated depth interval of any given well (*16*, *45*). The small study area considered here is topographically flat, dominated by unsaturated zone rather than riverine recharge [(as suggested by higher $^{18}O/^{16}O$ and $^{2}H/^{1}H$ than potential river sources; (*63*)] and consists exclusively of interconnected unconfined aquifers (*54*). The PEM model requires an estimate of the ratio, *n*, between total volume and sampled volume for each well. Here we estimate *n* (Table S1) as:

$$n = \frac{d_{max} - d_{WT}}{d_{max} - d_{min}} \qquad \text{(S4)}$$

where d_{max}, d_{min}, and d_{WT} refer to the maximum screened depth, minimum screened depth, and water-table depth, respectively. We assume a pre-industrial mean water table depth of 8 m (*64*). For a given n, the PEM residence time distribution $g(t)$ is a function of only one unknown variable, τ:

$$g(t) = \frac{n}{\beta\tau} e^{\frac{t}{\beta\tau}} \text{ for } t \geq \beta \ln(n);\ g(t) = 0 \text{ for } t < \beta \ln(n);\ \beta = \left(1 - \ln\left(\frac{1}{n}\right)\right) \qquad \text{(S5)}$$

Using the PEM model, we take the following approach to estimate Γ and $g(t)$. First, using equation S4 to calculate n, we estimate τ by maximizing agreement between PEM-simulated and measured inert age tracers. For wells 180-1, 170, and 183 (which were ^{3}H and ^{85}Kr free, within error), ^{39}Ar was used to estimate τ. For wells 180-2 and 180-3 (which had detectable ^{3}H and ^{85}Kr but were not measured for ^{39}Ar), ^{85}Kr was used for this purpose. (We do not attempt this exercise for well 180-4, because samples from this well were free of ^{85}Kr and ^{3}H, but ^{39}Ar was not measured and thus we lacked an intermediate age constraint.) Next, we compared ^{14}C and ^{3}H activities predicted by the PEM model (constrained by n and inert tracer-derived τ) to observations. Whereas simulated ^{3}H displayed close agreement with observations in the ^{3}H-free deeper wells, measured ^{14}C activities were found to fall systematically below simulated activities if $^{14}C_0$ was assumed equal to $^{14}C_{atm}$ (Γ=1). We tuned $^{14}C_0$ in the model by changing Γ to maximize agreement with observed ^{14}C. Figure S3 shows well-specific residence time distributions and comparisons of PEM-simulated and measured tracer activities. Table S2 shows a comparison for mean age (τ) estimates of the three deeper wells for which ^{39}Ar was measured between PF and PEM age ranges based either on ^{39}Ar or uncorrected ^{14}C (i.e. Γ=1).

Table S2. Simulated mean age ranges (τ) based solely on either ^{39}Ar or uncorrected ^{14}C (Γ=1) using both the PF (i.e. neglecting mixing) and PEM models. Under both models, ^{39}Ar-derived ages are an order of magnitude younger than uncorrected ^{14}C-derived ages.

Well Identification				**PF τ range (yr)**		**PEM τ range (yr)**	
USGS Station ID	*GAMA ID*	*NAWQA ID (CVAL-)*	*Alt ID*	^{39}Ar	^{14}C (Γ=1)	^{39}Ar	^{14}C (Γ=1)
364200119420001	KINGFP-02	ETN1-01	180-1	500-674	5813-6154	565-790	6800-7247
364156119475201	KING-17	PAS1-18	170	489-657	2949-3188	594-840	3191-3494
364239119440901	KINGFP-03	ETN1-183	183	231-308	7211-6824	240-324	7878-8338

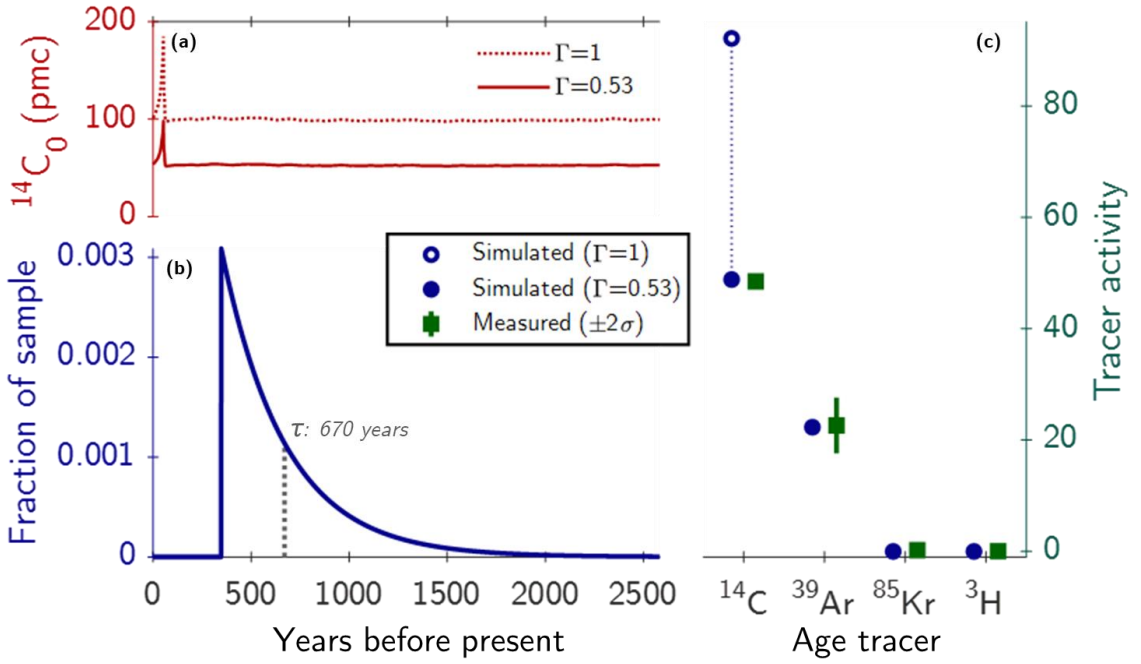

Figure S3.1 (*reprint of Figure 2*)**.** Well 180-1 estimation of initial ^{14}C activity (panel a) and groundwater residence-time distribution (*g(t)*, panel b) via evaluation of PEM-simulated versus measured tracer activity (panel c). Tracer activity (panel c) is shown in units of pmC, pmAr, dpm cc^{-1}, and TU for ^{14}C, ^{39}Ar, ^{85}Kr, and ^{3}H, respectively. Open and closed circles (panel c) show PEM-simulated ^{14}C activity associated with atmospheric (Γ=1) and sub-atmospheric (Γ<1) $^{14}C_0$, respectively.

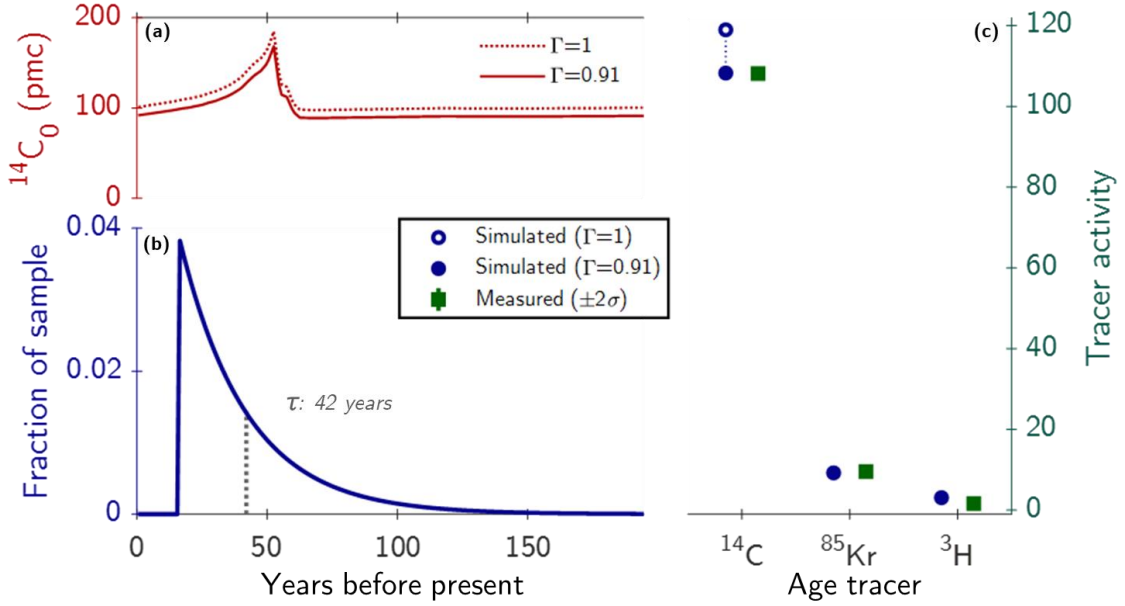

Figure S3.2. Well 180-2 estimation of initial ^{14}C activity (panel a) and groundwater residence-time distribution (*g(t)*, panel b) via evaluation of PEM-simulated versus measured tracer activity (panel c). Tracer activity (panel c) is shown in units of pmC, pmAr, dpm cc^{-1}, and TU for ^{14}C, ^{39}Ar, ^{85}Kr, and ^{3}H, respectively. Open and closed circles (panel c) show PEM-simulated ^{14}C activity associated with atmospheric (Γ=1) and sub-atmospheric (Γ<1) $^{14}C_0$, respectively.

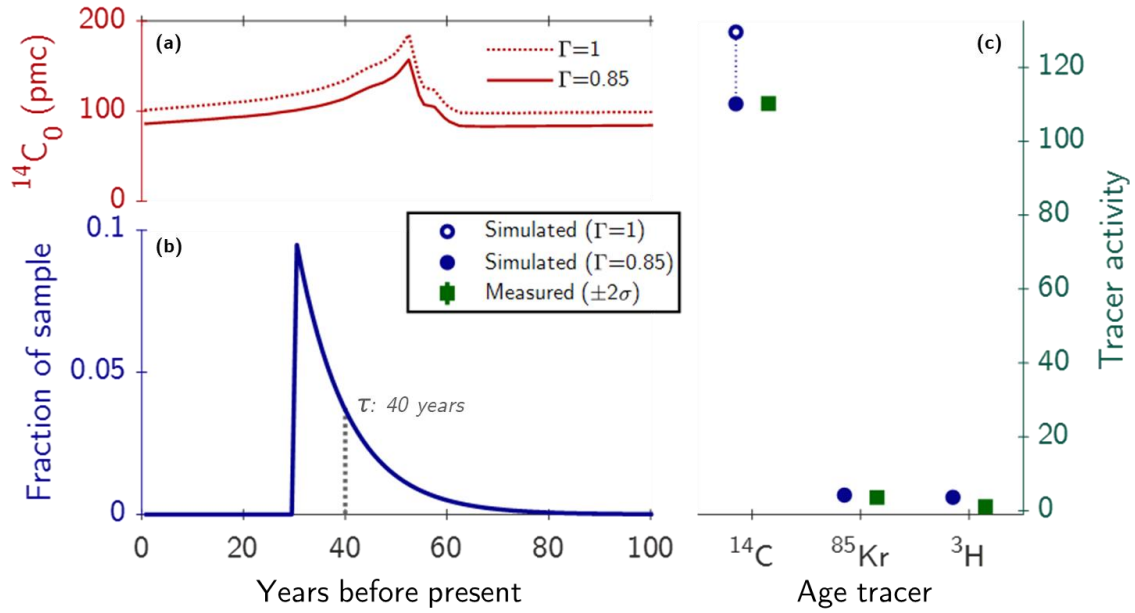

Figure S3.3. Well 180-3 estimation of initial ^{14}C activity (panel a) and groundwater residence-time distribution (*g(t)*, panel b) via evaluation of PEM-simulated versus measured tracer activity (panel c). Tracer activity (panel c) is shown in units of pmC, pmAr, dpm cc^{-1}, and TU for ^{14}C, ^{39}Ar, ^{85}Kr, and ^{3}H, respectively. Open and closed circles (panel c) show PEM-simulated ^{14}C activity associated with atmospheric (Γ=1) and sub-atmospheric (Γ<1) $^{14}C_0$, respectively.

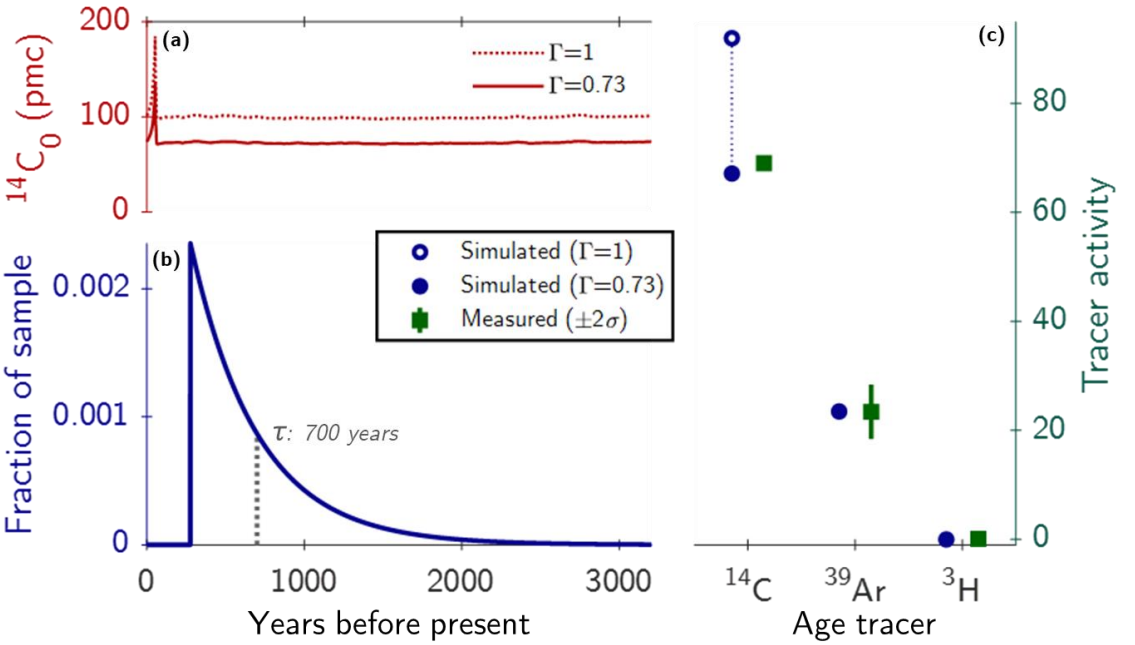

Figure S3.4. Well 170 estimation of initial ^{14}C activity (panel a) and groundwater residence-time distribution (*g(t)*, panel b) via evaluation of PEM-simulated versus measured tracer activity (panel c). Tracer activity (panel c) is shown in units of pmC, pmAr, dpm cc^{-1}, and TU for ^{14}C, ^{39}Ar, ^{85}Kr, and ^{3}H, respectively. Open and closed circles (panel c) show PEM-simulated ^{14}C activity associated with atmospheric (Γ=1) and sub-atmospheric (Γ<1) $^{14}C_0$, respectively.

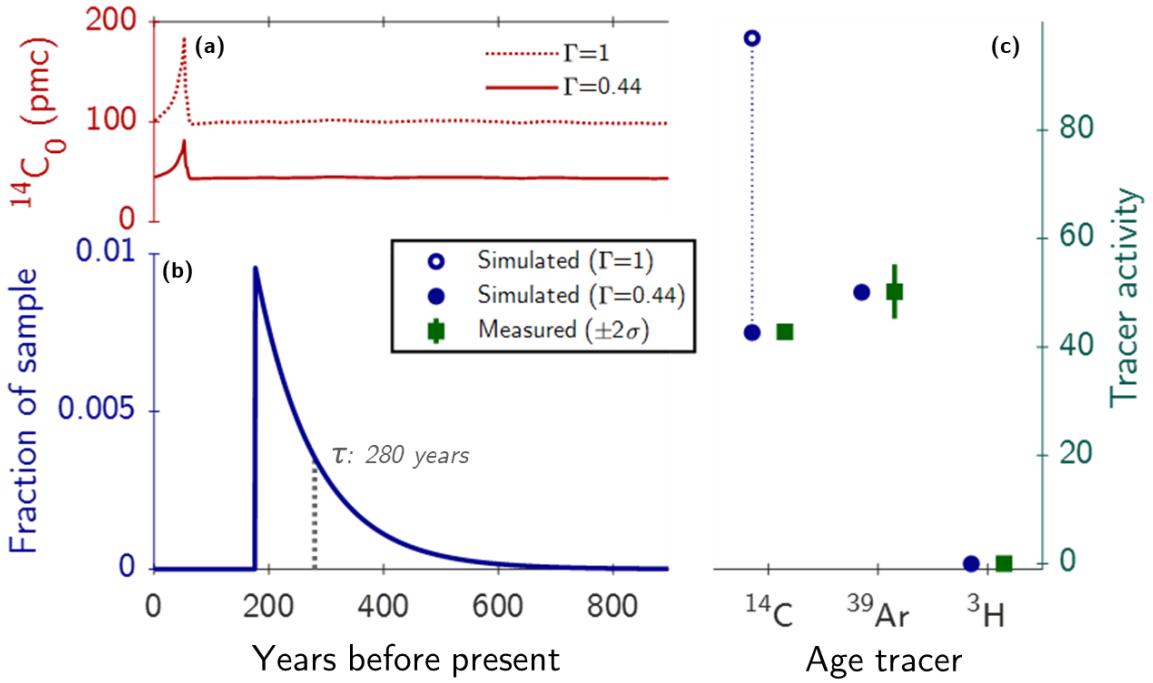

Figure S3.5. Well 183 estimation of initial ^{14}C activity (panel a) and groundwater residence-time distribution (*g(t)*, panel b) via evaluation of PEM-simulated versus measured tracer activity (panel c). Tracer activity (panel c) is shown in units of pmC, pmAr, dpm cc^{-1}, and TU for ^{14}C, ^{39}Ar, ^{85}Kr, and ^{3}H, respectively. Open and closed circles (panel c) show PEM-simulated ^{14}C activity associated with atmospheric (Γ=1) and sub-atmospheric (Γ<1) $^{14}C_0$, respectively.

By comparing τ and Γ with depth, several key trends emerge. First, τ increases with mean screened depth (i.e. the center depth of the screened interval for each well), and wells with similar mean screened depths have similar τ (e.g. 180-2 & 180-3 and 180-1 & 170). By comparison, relative age estimates based on ^{14}C in the absence of ^{39}Ar data would suggest a several-thousand year difference in τ between well 180-1 (^{14}C = 48.5 pmC, mean screened depth = 157 m) and well 170 (^{14}C = 69.0 pmC, mean screened depth = 148 m), whereas our PEM model approach constrained by ^{39}Ar yields consistent τ within several decades. Second, Γ is considerably higher for shallower and younger groundwater than it is for deeper and older groundwater, although we emphasize again here that wells with screened intervals in the 50-100 m depth range likely represent bimodal mixtures between modern and pre-development groundwater (*16*). We suggest that this trend in Γ primarily results from a mid-20th century shift towards greater DIC system openness (SI-2). Indeed, we find an expected negative correlation between inferred Γ and pH for these five wells. We note however that the variably open-system DIC model does not fully account for the low value of Γ in well 183 (0.44), which yields $^{14}C_0$ of ~44 pmC falling several pmC below the fully closed-system expectation ~50 pmC, for pre-1950s recharge. One plausible candidate mechanism for additional lowering of $^{14}C_0$ beyond closed-system dissolution is respiration of old organic matter by soil microbes. We speculate that whereas post-1950s recharge may readily carry modern, surface-derived organic carbon to the unsaturated zone from agricultural runoff, pre-modern unsaturated zone CO_2 may have derived from several hundred-year old organic matter at depth. Nonetheless, we emphasize that system openness is the primary control on Γ but note that additional inert tracer measurements, ideally both ^{39}Ar and ^{85}Kr, are important for precisely constraining $^{14}C_0$. However, given the present cost and complexity of measuring these novel inert age tracers, investigating DIC parameters (total DIC content, pH, $\delta^{13}C$) in the context of system openness provides useful qualitive constraints on $^{14}C_0$.

Appendix S2: Idealized variably open-system DIC model

The idealized carbonate dissolution model presented in this study is designed to explore the relationships between groundwater DIC isotopic composition (^{14}C activity, $\delta^{13}C$), total DIC, pH, and alkaline Earth metal concentrations for varying system "openness" for a given soil pCO_2. The model evaluates the above-mentioned DIC system parameters at three conceptual stages, following a similar treatment to Clark & Fritz (1997): (1) the initial dissolution of soil CO_2 (before carbonate dissolution); (2) the point of isolation of shallow groundwater from soil CO_2; (3) closed-system equilibrium dissolution of carbonate minerals in the saturated zone. Below, we present graphical examples of DIC parameter evolution and describe and define the systems of equations solved at each stage. Figure S4 shows the variability of DIC and pH from stages 1-3 for a fixed soil pCO_2 of 2.1% (21000 µatm) at 20 ºC:

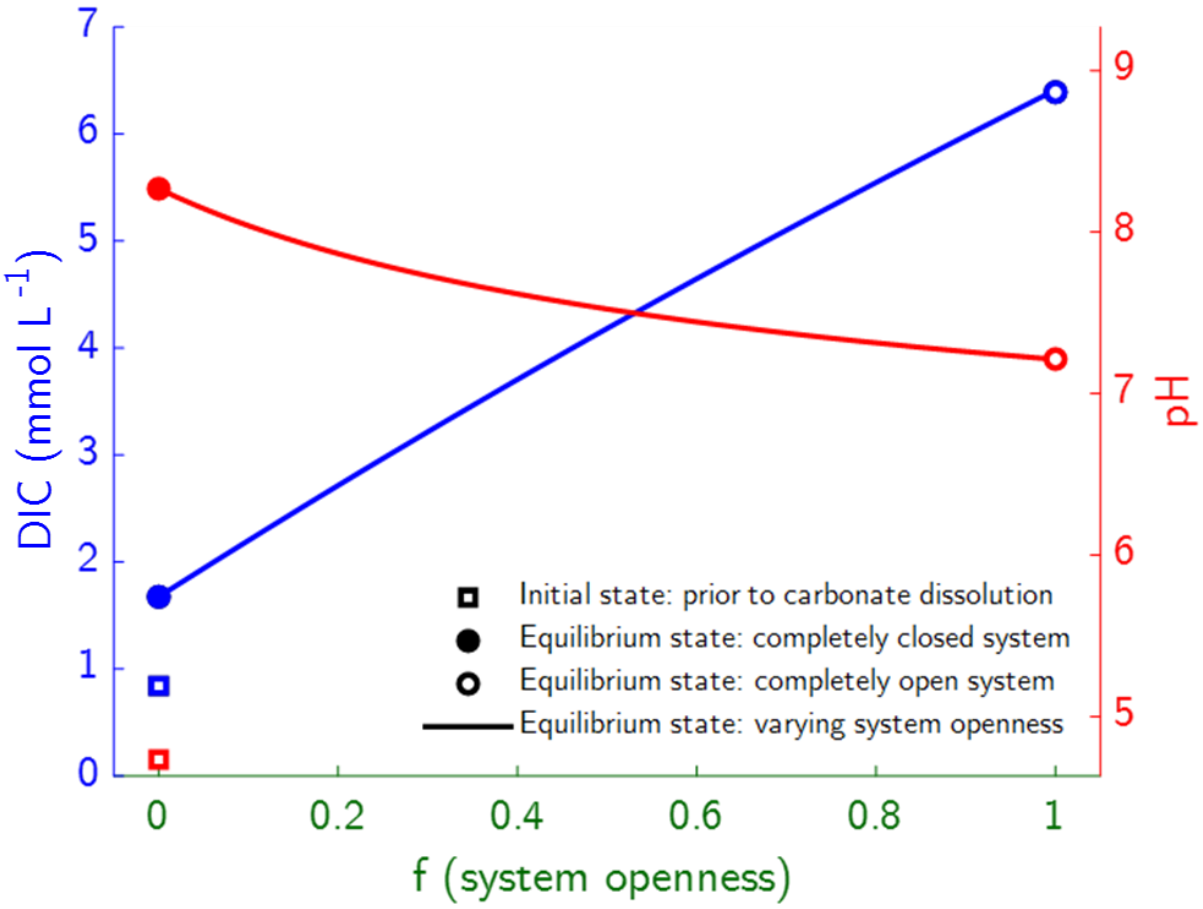

Figure S4. Model evolution of groundwater DIC and pH due to variably open and closed system dissolution of carbonate minerals. Initial DIC and pH (i.e. stage (1), when no carbonate has dissolved) are shown as open squares. Completely closed (open) system equilibrium values are shown as filled (open) circles, and equilibrium pH and DIC for varying degrees of open-system carbonate dissolution prior to isolation from soil CO_2 are shown as solid lines. Soil pCO_2 is fixed at 21000 µatm and pK_c is -7.98 in this example.

The first stage considers the equilibrium dissolution of soil CO_2 and its subsequent hydration in initially DIC-free water yielding $CO_{2(aq)}$, H^+, and HCO_3^-:

$$CO_{2(g)} + H_2O \leftrightharpoons H_2CO_3 \leftrightharpoons H^+ + HCO_3^- \qquad (S6)$$

We apply the hydration convention ($[CO_{2(aq)}^*] \approx [CO_{2(aq)}] + [H_2CO_3]$) to calculate the equilibrium concentration and speciation of DIC and pH as function of soil pCO_2:

$$DIC = [CO_{2(aq)}^*] + [HCO_3^-] + [CO_3^{2-}] \quad (S7)$$

$$[CO_{2(aq)}^*] = K_H pCO_2 \quad (S8)$$

$$[HCO_3^-] = \sqrt{K_1 K_H pCO_2} \quad (S9)$$

$$[CO_3^{2-}] = K_1 K_2 K_H pCO_2 \quad (S10)$$

$$pH = -\log_{10}([H^+]) = -\log_{10}(\sqrt{K_1 K_H pCO_2}) \quad (S11)$$

where all concentrations are given in mol L^{-1}, pCO_2 is given in μatm, and equilibrium constants K_1 and K_2 (*22*) and CO_2 Henry constant K_H (*65*) are prescribed for 20 °C freshwater. We define DIC_0 to be the equilibrium DIC at stage 1 calculated using equations S7-S11.

We next consider stage 2, the instantaneous point at which the system transitions from being open to closed (i.e. becoming isolated from overlying soil CO_2). Between stages 1 and 2, an additional amount of DIC ($DIC_{iso} - DIC_0$) has been added to the system by open-system carbonate and CO_2 dissolution. In our model, DIC_0 is prescribed directly for a given f value, by definition (equation 2). Because $[CO_{2(aq)}^*]$ remains unchanged from stage 1, we solve first for $[H^+]$ at stage 2 in terms of $[CO_{2(aq)}^*]$ and DIC_0 by minimizing the following equation using MATLAB's fminsearch function:

$$[CO_{2(aq)}^*]\left(\frac{K_1}{[H^+]} + \frac{K_1 K_2}{[H^+]^2} + 1\right) - TIC_0 = 0 \quad (S12)$$

The remaining unknown parameters can then be determined as a function of $[H^+]$:

$$[HCO_3^-] = K_1[CO_{2(aq)}^*]/[H^+] \quad (S13)$$

$$[CO_3^{2-}] = K_1 K_2[CO_{2(aq)}^*]/[H^+]^2 \quad (S14)$$

The amount of carbonate mineral ($MeCO_3$) dissolved prior to isolation, given by the dissolved concentration of alkaline Earth metals ($[Me^{2+}] = [Mg^{2+}] + [Ca^{2+}]$), can then be determined by dividing the gain in $[HCO_3^-]$ between stages 1 and 2 in half, according to the net reaction:

$$MeCO_3 + H_2CO_3 \rightarrow Me^{2+} + 2HCO_3^- \quad (S15)$$

For stage 3, we solve for the concentrations of DIC species, $[H^+]$, and $[Me^{2+}]$ for closed-system equilibrium dissolution of carbonate minerals:

$$H_2CO_3 + MeCO_{3(s)} \leftrightharpoons 2H^+ + 2CO_3^{2-} + Me^{2+} \leftrightharpoons 2HCO_3^- + Me^{2+} \quad (S16)$$

We reduce an original system of six equations and unknowns (first and second dissociations of carbonic acid, dissociation of water, dissolution of $MeCO_{3(s)}$, electroneutrality, conservation of inorganic carbon) to two equations and unknowns, solving for $[Me^{2+}]$ and $[HCO_3^-]$:

$$[Me^{2+}](2+[HCO_3^-]K_2/K_c) - (2K_c+K_wK_c/[HCO_3^-]K_2)/[Me^{2+}] - [HCO_3^-] = 0 \quad (S17)$$

$$K_2[Me^{2+}][HCO_3^-]^2/(K_1K_c) + [HCO_3^-] - [Me^{2+}] + K_c/[Me^{2+}] - DIC_{iso} + [Me^{2+}]_{iso} = 0 \quad (S18)$$

where K_c is the carbonate solubility product ($K_c \equiv [CO_3^{2-}][Me^{2+}]$) and the subscript "iso" refers to parameter values at the point of isolation (i.e. the instantaneous transition point from open to closed system conditions). The system of equations is solved using MATLAB's fsolve function and $[H^+]$ and $[CO_{2(aq)}^*]$ are subsequently determined based on $[Me^{2+}]$ and $[HCO_3^-]$:

$$[H^+] = [HCO_3^-][Me^{2+}]K_2/K_c \quad (S19)$$

$$[CO_{2(aq)}^*] = [H^+][HCO_3^-]/K_1 \quad (S20)$$

At this point, $[CO_3^{2-}]$ and DIC can be determined via S14 and S7, respectively.
Finally, to define f (Eq. 2), we must determine parameter values for open-system equilibrium carbonate dissolution:

$$CO_{2(g)} + H_2O + MeCO_{3(s)} \leftrightharpoons H_2CO_3 + MeCO_{3(s)} \leftrightharpoons 2H^+ + 2CO_3^{2-} + Me^{2+} \leftrightharpoons 2HCO_3^- + Me^{2+} \quad (S21)$$

To do this, we follow the same procedure as in stage 3, except that $[CO_{2(aq)}^*]$ is fixed at its solubility equilibrium concentration with soil CO_2 (equation S8). Thus, for open-system equilibrium, the system can be reduced to a single equation and unknown and solved numerically for $[H^+]$:

$$2K_c[H^+]^2/(pCO_2K_1K_2K_H) + [H^+] - K_w/[H^+] - 2pCO_2K_1K_2K_H/[H^+]^2 - pCO_2K_1K_H/[H^+]^2 = 0 \quad (S22)$$

The equilibrium open-system DIC ($DIC_{eq,open}$ in the definition of f, equation 2) is then given by:

$$DIC_{eq,open} = pCO_2K_H\,(1 + K_1/[H^+] + K_1K_2/[H^+]^2) \quad (S23)$$

In stages 1 and 2, where shallow groundwater is exposed to soil CO_2 under open-system conditions, the isotopic composition of DIC is simulated by determining the speciation of DIC and applying equilibrium fractionation factors (*24, 66–68*) for HCO_3^- and $CO_{2(aq)}$ relative to soil $CO_{2(g)}$ in 20 ºC freshwater. In stage 3, any additional DIC added by closed-system dissolution is assumed to carry the carbon isotopic signature of carbonate minerals. Therefore, we define open-system and closed-system values for $\delta^{13}C$ and $\Delta^{14}C$ (which we convert to ^{14}C activity in pmC) in the following way. First, for open-system dissolution at isotopic equilibrium between DIC and soil CO_2, we approximate the carbon isotopic composition of groundwater as being offset from the isotopic composition soil CO_2 by the weighted mean of equilibrium fractionation factors between $CO_{2(aq)}$, HCO_3^-, and soil CO_2. The equilibrium fractionation ε values (for $^{13}C/^{12}C$), $\varepsilon_{a\text{-}g}$ and $\varepsilon_{b\text{-}g}$, are defined:

$$\varepsilon_{a\text{-}g} = \delta^{13}C_{CO2,aq} - \delta^{13}C_{CO2,soil} \quad (S24)$$
$$\varepsilon_{b\text{-}g} = \delta^{13}C_{HCO3} - \delta^{13}C_{CO2,soil} \quad (S25)$$

where $\delta^{13}C_{CO2,aq}$, $\delta^{13}C_{HCO3,}$ and $\delta^{13}C_{CO2,soil}$ refer to the $\delta^{13}C$ of dissolved CO_2, dissolved bicarbonate, and gaseous soil CO_2, respectively. The open-system carbon isotopic composition of DIC is therefore given by:

$$\delta^{13}C_{open} = \delta^{13}C_{CO2,soil} + \varepsilon_{a\text{-}g}([CO_{2(aq)}^*]/DIC) + \varepsilon_{b\text{-}g}([HCO_3^-]/DIC) \quad (S26)$$

Because the definition of $\Delta^{14}C$ partially accounts for mass-dependent equilibrium fractionation, the net equilibrium fractionation of $\Delta^{14}C$ is ~0.2ε, and so to several tenths of 1 pmC, equilibrium fractionation is negligible for $\Delta^{14}C$. Thus, we simply by approximating open-system $\Delta^{14}C$ as:

$$\Delta^{14}C_{open} = \Delta^{14}C_{CO2,soil} \quad (S27)$$

Because there is no subsequent gas exchange (and, consequentially, no isotopic equilibration) between DIC and CO_2 after isolation, the $\Delta^{14}C$ and $\delta^{13}C$ of DIC acquired by closed-system dissolution is simply equal to the $\Delta^{14}C$ and $\delta^{13}C$ of carbonates in the saturated zone:

$$\delta^{13}C_{closed} = \delta^{13}C_{carb} \quad (S28)$$
$$\Delta^{14}C_{closed} = \Delta^{14}C_{carb} \quad (S29)$$

The model solves for final groundwater $\delta^{13}C$ and $\Delta^{14}C$ as a function of system openness in the following manner. Because the amount of total DIC acquired under open-system conditions is equal to DIC_{iso}, any remaining DIC acquired via closed-system dissolution is equal to $DIC-DIC_{iso}$. Thus, the final $\delta^{13}C$ and $\Delta^{14}C$ of groundwater after isolation from soil CO_2 and addition of any carbon via closed-system dissolution is given by:

$$\delta^{13}C_{final} = (DIC_{iso}/DIC)\delta^{13}C_{open} + (1-DIC_{iso}/DIC)\delta^{13}C_{closed} \quad (S30)$$
$$\Delta^{14}C_{final} = (DIC_{iso}/DIC)\Delta^{14}C_{open} + (1-DIC_{iso}/DIC)\Delta^{14}C_{closed} \quad (S31)$$

Consider, for example, the case of entirely open-system dissolution (f=1). In this case, $DIC_{iso}=DIC_{eq,open}=DIC$ (by definition, Eq. 2) and thus $\delta^{13}C_{final}= \delta^{13}C_{open}$ and $\Delta^{14}C_{final} = \Delta^{14}C_{open}$. For the case of entirely closed-system dissolution (f=0), $DIC_{iso}=DIC_0$ and DIC equals approximately twice DIC_0 at closed-system equilibrium (e.g. Figure S4). Therefore, $\delta^{13}C_{final} = 0.5*\delta^{13}C_{open} + 0.5*\delta^{13}C_{closed}$ and $\Delta^{14}C_{final} = 0.5*\Delta^{14}C_{open} + 0.5*\Delta^{14}C_{closed}$. If $\delta^{13}C_{closed} = 0‰$ and $\Delta^{14}C_{closed} = 0$ pmC (typical value), then the effect of closed-system carbonate dissolution will be to dilute $\delta^{13}C$ and $\Delta^{14}C$ each by one half.

Figure S5 shows the simulated relationship between $\delta^{13}C$ and f as well as measured and simulated relationships between $\delta^{13}C$ and ^{14}C for varying soil and carbonate mineral endmember isotopic compositions. We note that the predicted variability in $\delta^{13}C$ between fully open and fully closed conditions for a given set of endmember values (e.g. dashed green line in Figure S5) is small (3-4‰) relative to the range of potential endmember $\delta^{13}C$ values (~10‰, Clark & Fritz, 1997). We suggest that spatiotemporal variability in $\delta^{13}C$, perhaps due to changes in soil biogeochemistry driven by agricultural pollution, obfuscates the smaller predicted inverse relationship between $\delta^{13}C$ and system openness. This stands in contrast to the remarkably consistent relationship between ^{14}C and pH (or $CO_{2(aq)}$/DIC), which operates in the same sense as our model predicts (Figures 1 and 3). $\delta^{13}C$ measurements still do provide a useful qualitative constraint on the manner of isotopic equilibration, indicating that soil CO_2-DIC isotopic equilibration is likely attained under open-system conditions but carbonate mineral-DIC equilibrium under closed-system conditions is not. To demonstrate this, we note that the expected open-system DIC $\delta^{13}C$ for pH ~7.5 is ~+7.5‰ relative to soil CO_2 ($CO_{2(aq)}$ and HCO_3^- represent ~10% and 90% of DIC and their equilibrium isotopic enrichments relative to soil CO_2 at 20 ºC are -1.1‰ and +8.5‰, respectively). All groundwater $\delta^{13}C$ measurements for which ^{14}C activity is greater than 100 pmC fall between -16.5 and -13.5‰, consistent with soil CO_2 $\delta^{13}C$ between ~-24 and -21‰ for open-system isotopic equilibrium. This range falls well within the literature range for microbial respiration of soil organic carbon derived from C_3 plants (*22*). Conversely, if isotopic equilibrium in the saturated zone between DIC and carbonate minerals were attained, $\delta^{13}C$ and ^{14}C of groundwater would be close carbonate mineral values (-5 to 5‰ and 0 pmC, respectively; Clark & Fritz, 1997), since equilibrium fractionation between HCO_3^- and $CaCO_3$ or $MgCO_3$ at 20 ºC is small (<1‰). Given that terrestrial carbonate $\delta^{13}C$ may even fall below this -5‰ value [e.g. (*20*)], the interpretation of the small range of open-system versus closed-system $\delta^{13}C$ signals, in light of large end-member uncertainties, is challenging and greatly limits the use of $\delta^{13}C$ for this study.

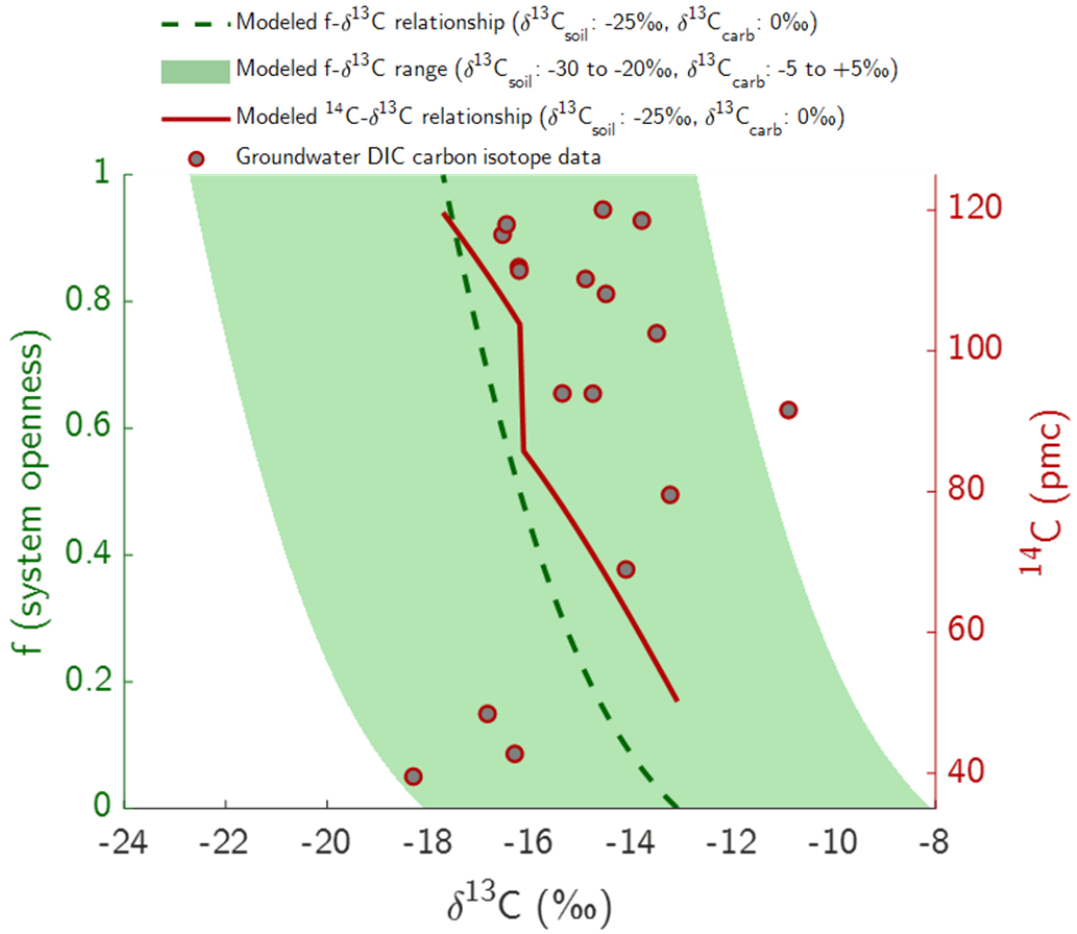

Figure S5. Modeled relationship between f (left axis) and $\delta^{13}C$ and ^{14}C (right axis) and $\delta^{13}C$ for varying endmember groundwater $\delta^{13}C$ composition. Dashed green line shows modeled f-$\delta^{13}C$ relationship for conventional endmember composition (soil $\delta^{13}C$: -25‰, carbonate $\delta^{13}C$: 0‰). Shaded green region shows expected range of $\delta^{13}C$ associated with f between 0 and 1 for soil $\delta^{13}C$ between -30 and -20‰ and carbonate $\delta^{13}C$ between -5 and +5‰. Solid maroon line shows modeled relationship between ^{14}C and $\delta^{13}C$ for conventional endmember $\delta^{13}C$ composition and $^{14}C_0$ of 120 (100) pmC for f greater (less) than 0.5. Grey circles indicate actual groundwater DIC measurements in this study.

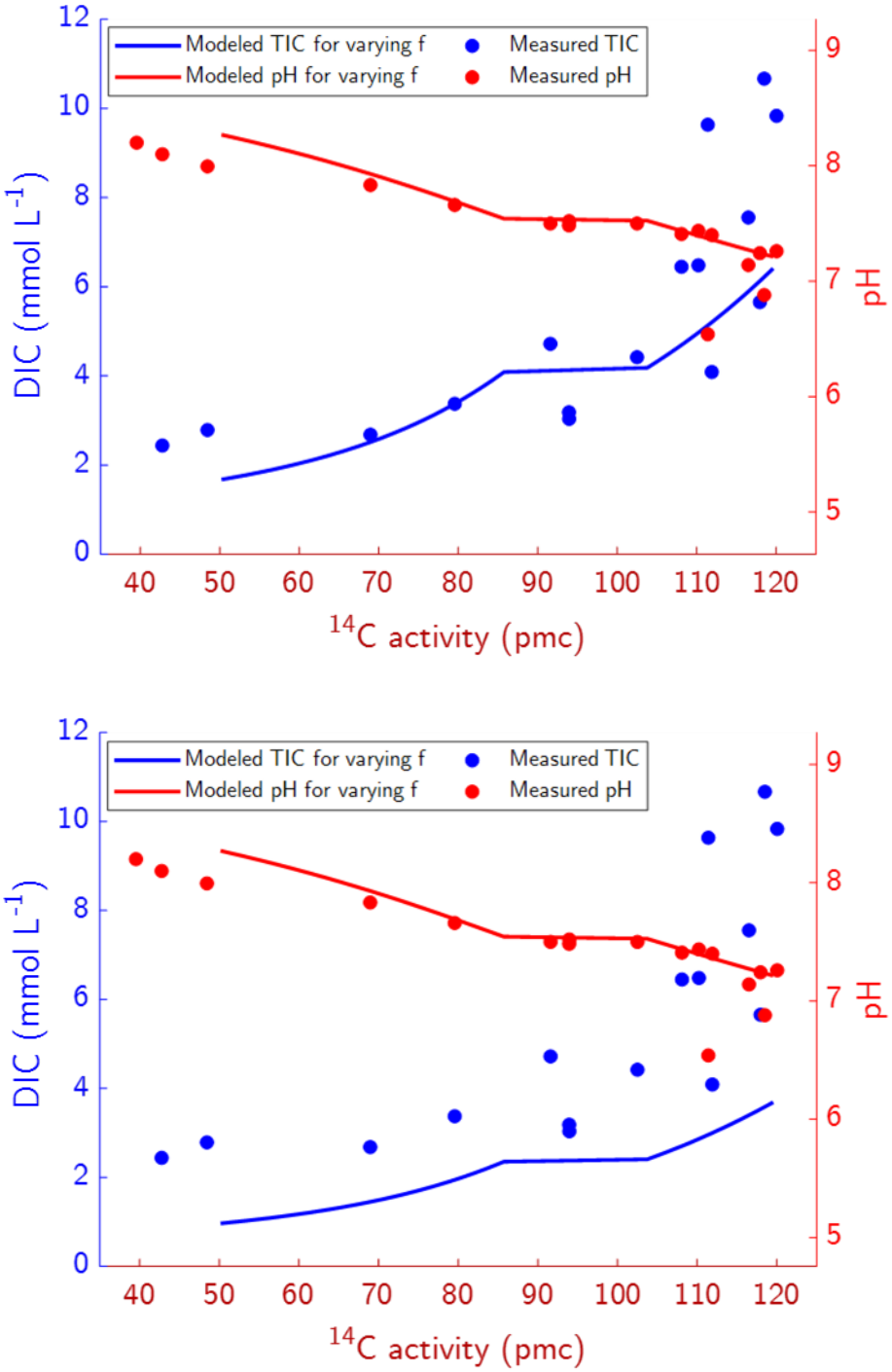

Figure S6. Modeled relationships between DIC, ^{14}C activity and pH. **(a-top)** Modeled and measured **DIC** and pH vs ^{14}C activity in groundwater. The model assumes fixed soil pCO_2 and pK_c of 21000 µatm and 7.97, respectively, and sets $^{14}C_{soil}$ equal to 120 pmC for f>0.5 and 100 pmC for f<0.5; **(b-bottom)** Modeled and measured **DIC** and pH vs ^{14}C activity in groundwater. The model here prescribes fixed soil pCO_2 and pK_c of 12000 µatm and 8.45, respectively, and sets $^{14}C_{soil}$ equal to 120 pmC for f>0.5 and 100 pmC for f<0.5.

Whereas the model suggests a weak sensitivity of $\delta^{13}C$ to system openness relative to potential variability in endmember composition, both the model and data display a strong relationship between ^{14}C and pH as well as ^{14}C and DIC, giving confidence to the notion that the primary control on ^{14}C activities in this system is DIC-system openness rather than radioactive decay (Figure S6a). While the sense of the relationships between f, ^{14}C, DIC, and pH in the model are independent of soil pCO_2 and carbonate solubility (K_c) – i.e. higher ^{14}C and DIC and lower pH

for higher f – the absolute values are not. In Figure S6a (and in Figure 3), we present a plausible combination of soil pCO_2 and K_c that explains much of the observed variability in our groundwater measurements. In this scenario, soil pCO_2 is 2.1% (21000 μatm), a typical value for warm regions (*22*) and K_c is $10^{-7.97}$, which is higher than the pure calcite value at 20 ºC ($10^{-8.45}$). Figure S6b shows another example in which soil pCO_2 is set to 12000 μatm and the pure calcite K_c value is used. While the ^{14}C-pH relationship is well represented in both cases, the latter case (Figure S6b) systematically underestimates DIC. We suspect that the true mean carbonate solubility in this system is higher than that of pure calcite, perhaps due to the high magnesium content of carbonate minerals. Magnesium-rich carbonates have considerably higher solubilities than pure calcite [e.g. magnesite has pK_c of 7.8 at 25 °C (*69*)], and magnesite is known to be abundant in the Kings River region. Mg^{2+}/Ca^{2+} is high (>0.5 molar ratio) in all samples considered in this study.

However, we also emphasize here that this idealized model only considers carbonate dissolution, and other sources of DIC, such as silicate weathering, may be important. Additionally, soil amendments containing alkaline Earth metals (gypsum, for example) may contribute Mg^{2+} and Ca^{2+}, affecting their dissolved ratios in groundwater. Further, precipitation and redissolution of carbonates, especially from modern groundwater impacted by input of soil amendments, is a potentially important process not captured by this idealized model. We therefore reiterate that this model is intended solely as a qualitative tool to demonstrate a common mechanism positively linking ^{14}C with DIC and negatively linking ^{14}C with pH. While we do not attempt to conclusively specify an f value associated with each well in this study, we provide examples values (in an instructional sense only) in the Supplementary Data Set for pCO_2 = 2.1% and pK_c = -7.98.

One potentially important concern for the interpretation of measured groundwater ^{14}C in the context of this idealized model is the impact of mixing of different water masses, which may have experienced different extents of open and closed system dissolution. Many wells have long screened intervals (Figures S5-S6) that allow for broad mixture of groundwater ages, including mixing of pre-development and post-development waters. While the subject of mixing is addressed directly in SI-1, here we briefly consider the impact of mixing on the interpretation of DIC parameters in the context of this idealized variably open-system model. In Figure S7, we show modeled ^{14}C and DIC for f values between 0 and 1 alongside admixture-resultant ^{14}C and DIC from various degrees of binary mixing between groundwaters characterized by fully open and fully closed systems (i.e., f=0 and f=1, respectively). Even for this most extreme possible mixing scenario, ^{14}C resulting from mixing only slightly deviates from the actual model. For example, consider the difference between an equal parts mixture of f=0 and f=1 groundwater with the simulated values for f=0.5 (i.e., groundwater that became isolated from CO_2 after half the open-system equilibrium DIC had been obtained by vadose zone dissolution). In this case, the ^{14}C activity predicted by the model is ~86.5 pmC whereas the equal parts admixture of f=0 and f=1 water yields a ^{14}C activity of ~88.4 pmC. Conveniently, therefore, we expect that actual mixed groundwater samples will still plot closely along the modeled line, to within several pmC. In other words, the model closely approximates bulk f values, independent of mixing.

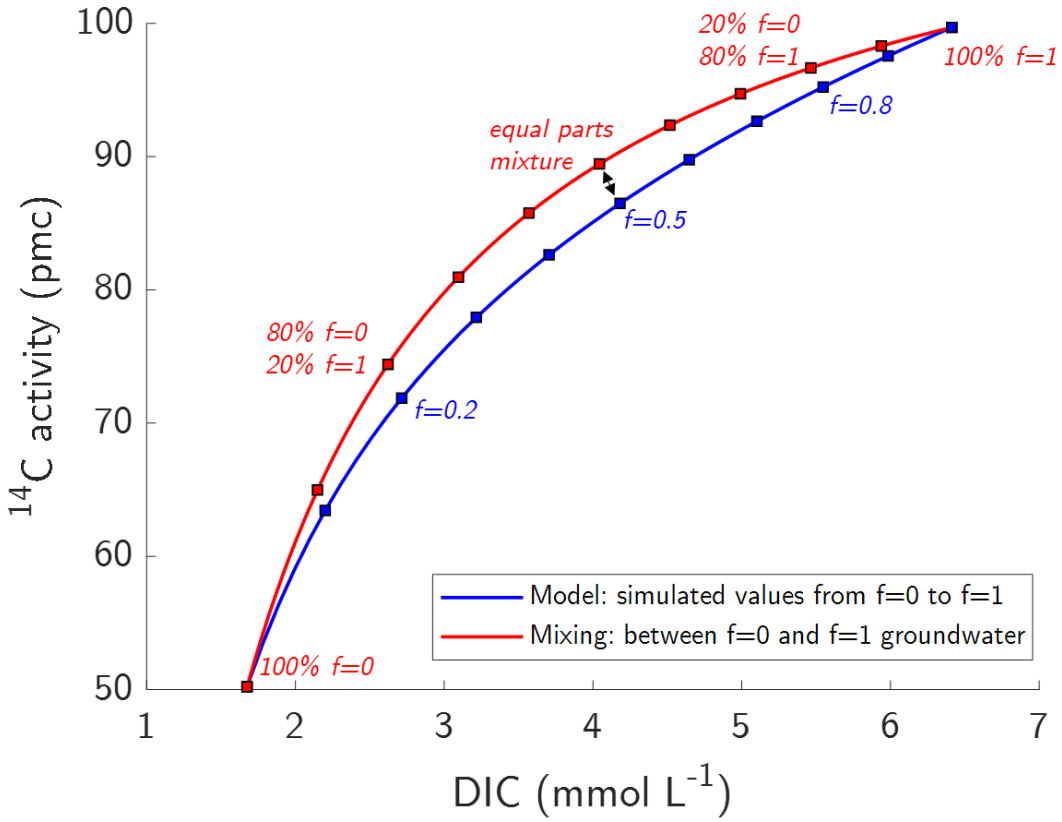

Figure S7: Comparison of mixing vs model prediction for ^{14}C activity and DIC in groundwater. In this example, f=0 and f=1 endmembers are mixed to various extents (red curve, squares indicate 10%-spaced mixture extents). The modeled curve is shown for comparison, with blue squares indicating 0.1-step changes in f.

Appendix S3: Soil CO_2-DIC Isotopic Equilibration Timescale

To estimate the timescale of isotopic equilibration between DIC at the water table with overlying soil CO_2, we make use of the well-established air-sea gas exchange equations (e.g., those presented in (*70*)) and consider an idealized example in which the upper one meter of groundwater exchanges carbon isotopes with CO_2 in overlying soil air. For this example we assume that DIC derived from carbonate mineral dissolution is initially ^{14}C free but gains ^{14}C via equilibration with soil CO_2, which we assume to have a modern atmospheric ^{14}C activity (assumed stationary in time due to the rapid soil CO_2 production and diffusive gas-phase equilibration timescales). Following (*70*), we define the e-folding isotopic equilibration timescale of DIC (τ_{14C}) for air-water gas exchange as:

$$\tau_{14C} = hR/G \qquad \text{(S32)}$$

where h is an effective diffusion length scale (i.e., 1 meter in this idealized case), R is the ratio of DIC to $CO_{2(aq)}$*, and G is a gas transfer velocity. To gain an order-of-magnitude estimate, here we simply consider a zero-wind G value of 1 m day^{-1} and calculate R using the equations and K1 and K2 equilibrium constants in Appendix S2, which yields a value of ~14. Plugging these values into equation S32, we obtain an e-folding timescale of ~14 days. We note that this idealized scenario may overestimate the appropriate diffusive length scale, given that substantial equilibration between CO_2 and DIC likely occurs in small pores in the vadose zone with radii much smaller than 1 meter (in which case our τ_{14C} estimate would be too long), but that diffusive gas exchange in the quiescent vadose zone may occur with a slower gas transfer velocity (in which case our τ_{14C} estimate would be too short). We suggest that this is estimate is likely valid to within an order of magnitude.

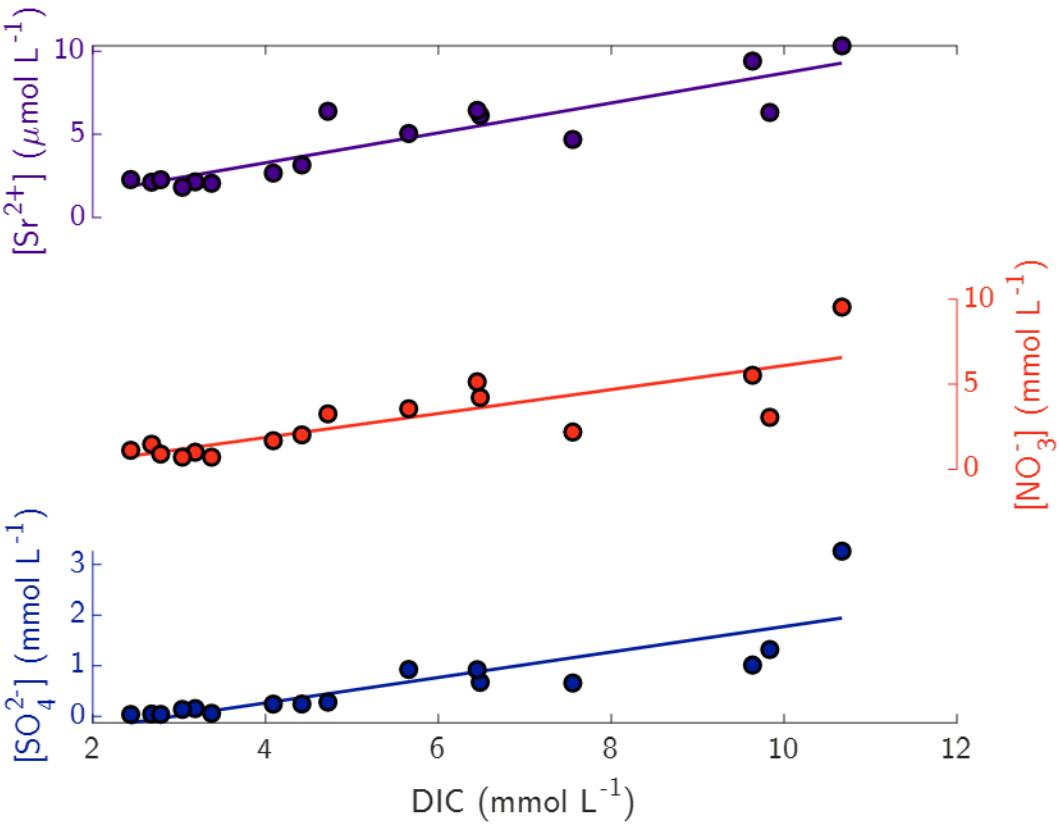

Figure S8. Groundwater strontium, nitrate, and sulfate concentrations versus DIC in the main study area. Positive correlations support inference of agricultural contamination and carbonate (lime) addition.

REFERENCES AND NOTES

1. B. L. Morris, A. R. L. Lawrence, P. J. C. Chilton, B. Adams, R. C. Calow, B. A. Klinck, *Groundwater and Its Susceptibility to Degradation: A Global Assessment of the Problem and Options for Management* (United Nations Environment Programme, 2003), p. 126.

2. M. Giordano, Global groundwater? Issues and solutions. *Annu. Rev. Env. Resour.* **34**, 153–178 (2009).

3. S. Siebert, J. Burke, J. M. Faures, K. Frenken, J. Hoogeveen, P. Döll, F. T. Portmann, Groundwater use for irrigation – a global inventory. *Hydrol. Earth Syst. Sci.* **14**, 1863–1880 (2010).

4. T. Gleeson, K. M. Befus, S. Jasechko, E. Luijendijk, M. B. Cardenas, The global volume and distribution of modern groundwater. *Nat. Geosci.* **9**, 161–167 (2016).

5. K. M. Befus, S. Jasechko, E. Luijendijk, T. Gleeson, M. Bayani Cardenas, The rapid yet uneven turnover of Earth's groundwater. *Geophys. Res. Lett.* **44**, 5511–5520 (2017).

6. S. Jasechko, D. Perrone, K. M. Befus, M. Bayani Cardenas, G. Ferguson, T. Gleeson, E. Luijendijk, J. J. McDonnell, R. G. Taylor, Y. Wada, J. W. Kirchner, Global aquifers dominated by fossil groundwaters but wells vulnerable to modern contamination. *Nat. Geosci.* **10**, 425–429 (2017).

7. J. Schewe, J. Heinke, D. Gerten, I. Haddeland, N. W. Arnell, D. B. Clark, R. Dankers, S. Eisner, B. M. Fekete, F. J. Colón-González, S. N. Gosling, H. Kim, X. Liu, Y. Masaki, F. T. Portmann, Y. Satoh, T. Stacke, Q. Tang, Y. Wada, D. Wisser, T. Albrecht, K. Frieler, F. Piontek, L. Warszawski, P. Kabat, Multimodel assessment of water scarcity under climate change. *Proc. Natl. Acad. Sci. U.S.A.* **111**, 3245–3250 (2014).

8. R. G. Taylor, B. Scanlon, P. Döll, M. Rodell, R. van Beek, Y. Wada, L. Longuevergne, M. Leblanc, J. S. Famiglietti, M. Edmunds, L. Konikow, T. R. Green, J. Chen, M. Taniguchi, M. F. P. Bierkens, A. M. Donald, Y. Fan, R. M. Maxwell, Y. Yechieli, J. J. Gurdak, D. M. Allen, M. Shamsudduha, K. Hiscock, P. J.-F. Yeh, I. Holman, H. Treide, Ground water and climate change. *Nat. Clim. Change* **3**, 322–329 (2013).

9. C. Dalin, Y. Wada, T. Kastner, M. J. Puma, Groundwater depletion embedded in international food trade. *Nature* **543**, 700–704 (2017).

10. B. R. Scanlon, C. C. Faunt, L. Longuevergne, R. C. Reedy, W. M. Alley, V. L. McGuire, P. B. McMahon, Groundwater depletion and sustainability of irrigation in the US High Plains and Central Valley. *Proc. Natl. Acad. Sci. U.S.A.* **109**, 9320–9325 (2012).

11. G. Ferguson, M. O. Cuthbert, K. Befus, T. Gleeson, J. C. McIntosh, Rethinking groundwater age. *Nat. Geosci.* **13**, 592–594 (2020).

12. F. Ritterbusch, S. Ebser, J. Welte, T. Reichel, A. Kersting, R. Purtschert, W. Aeschbach-Hertig, M. K. Oberthaler, Groundwater dating with atom trap trace analysis of ^{39}Ar. *Geophys. Res. Lett.* **41**, 6758–6764 (2014).

13. Z. T. Lu, P. Schlosser, W. M. Smethie Jr, N. C. Sturchio, T. P. Fischer, B. M. Kennedy, R. Purtschert, J. P. Severinghaus, D. K. Solomon, T. Tanhua, R. Yokochi, Tracer applications of noble gas radionuclides in the geosciences. *Earth Sci. Rev.* **138**, 196–214 (2014).

14. J. A. Hansen, B. C. Jurgens, M. S. Fram, Quantifying anthropogenic contributions to century-scale groundwater salinity changes, San Joaquin Valley, California, USA. *Sci. Total Environ.* **642**, 125–136 (2018).

15. C. C. Faunt, M. Sneed, J. Traum, J. T. Brandt, Water availability and land subsidence in the Central Valley, California, USA. *Hydrgeol. J.* **24**, 675–684 (2016).

16. B. C. Jurgens, J. K. Böhlke, L. J. Kauffman, K. Belitz, B. K. Esser, A partial exponential lumped parameter model to evaluate groundwater age distributions and nitrate trends in long-screened wells. *J. Hydrol.* **543**, 109–126 (2016).

17. K. R. Burow, N. M. Dubrovsky, J. L. Shelton, Temporal trends in concentrations of DBCP and nitrate in groundwater in the eastern San Joaquin Valley, California, USA. *Hydrogeol. J.* **15**, 991–1007 (2007)

18. A. K. Williamson, D. E. Prudic, L. A. Swain, *Ground-Water Flow in the Central Valley, California* (US Geological Survey Profrofessinal Paper, 1401D, 1989).

19. C. C. Faunt, ,*Groundwater Availability of the Central Valley Aquifer, California* (U.S. Geological Survey Professional Paper, 1766, 2009), p. 225.

20. I. Cartwright, M. J. Currell, D. I. Cendón, K. T. Meredith, A review of the use of radiocarbon to estimate groundwater residence times in semi-arid and arid areas. *J. Hydrol.* **580**, 124247 (2020).

21. Q. Hua, M. Barbetti, A. Z. Rakowski, Atmospheric radiocarbon for the period 1950–2010. *Radiocarbon* **55**, 2059–2072 (2013).

22. I. Clark, P. Fritz, *Environmental Isotopes in Hydrogeology*, (CRC Press, Boca Raton, 1997).

23. J.-C. Fontes, J.-M. Garnier, Determination of the initial ^{14}C activity of the total dissolved carbon: A review of the existing models and a new approach. *Water Resour. Res.* **15**, 399–413 (1979).

24. L. F. Han, L. N. Plummer, Revision of Fontes & Garnier's model for the initial ^{14}C content of dissolved inorganic carbon used in groundwater dating. *Chem. Geol.* **351**, 105–114 (2013).

25. C. M. Bethke, T. M. Johnson, Groundwater age and groundwater age dating. *Annu. Rev. Earth Planet. Sci.* **36**, 121–152 (2008).

26. A. Suckow, The age of groundwater – Definitions, models and why we do not need this term. *Appl. Geochem.* **50**, 222–230 (2014).

27. J. L. McCallum, P. G. Cook, C. T. Simmons, Limitations of the use of environmental tracers to infer groundwater age. *Groundwater* **53**, 56–70 (2015).

28. P. J. Reimer, E. Bard, A. Bayliss, J. W. Beck, P. G. Blackwell, C. B. Ramsey, C. E. Buck, H. Cheng, R. L. Edwards, M. Friedrich, P. M. Grootes, T. P. Guilderson, H. Haflidason, I. Hajdas, C. Hatté, T. J. Heaton, D. L. Hoffmann, A. G. Hogg, K. A. Hughen, K. F. Kaiser, B. Kromer, S. W. Manning, M. Niu, R. W. Reimer, D. A. Richards, E. M. Scott, J. R. Southon, R. A. Staff, C. S. M. Turney, J. van

der Plicht, IntCal13 and Marine13 radiocarbon age calibration curves 0–50,000 years cal BP. *Radiocarbon* **55**, 1869–1887 (2013).

29. C. Wood, P. G. Cook, G. A. Harrington, K. Meredith, R. Kipfer, Factors affecting carbon-14 activity of unsaturated zone CO_2 and implications for groundwater dating. *J. Hydrol.* **519**, 465–475 (2014).

30. K. T. Meredith, L. F. Han, S. E. Hollins, D. I. Cendón, G. E. Jacobsen, A. Baker, Evolution of chemical and isotopic composition of inorganic carbon in a complex semi-arid zone environment: Consequences for groundwater dating using radiocarbon. *Geochim. Cosmochim. Acta* **188**, 352–367 (2016).

31. F. J. J. Pearson, B. B. Hanshaw, *Isotopes in Hydrology 1970* (International Atomic Energy Agency, Vienna, 1970), pp. 271–285; http://www.iaea.org/inis/collection/NCLCollectionStore/_Public/45/025/45025950.pdf.

32. E. Ingerson, F. J. J. Pearson, *Recent Researches in the Fields of Hydrosphere, Atmosphere and Nuclear Geochemistry* (Maruzen, Tokyo, Japan, 1964), pp. 263–283.

33. M. A. Tamers, Validity of radiocarbon dates on ground water. *Geophys. Surv.* **2**, 217–239 (1975).

34. W. G. Mook, *Interpretation of Environmental Isotope and Hydrochemical Data in Groundwater Hydrology* (International Atomic Energy Agency, Vienna, Austria, 1976), pp. 213–225.

35. L. N. Plummer, E. C. Prestemon, D. L. Parkhurst, *An Interactive Code (NETPATH) For Modeling Net Geochemical Reactions Along a Flow Path, Version 2.0* (Water Resources Investigations Report, 94-4169, 1994).

36. S. Jasechko, A. Lechler, F. S. R. Pausata, P. J. Fawcett, T. Gleeson, D. I. Cendón, J. Galewsky, A. N. LeGrande, C. Risi, Z. D. Sharp, J. M. Welker, M. Werner, K. Yoshimura, Late-glacial to late-Holocene shifts in global precipitation δ18O. *Clim. Past.* **11**, 1375–1393 (2015).

37. S. Jasechko, Partitioning young and old groundwater with geochemical tracers. *Chem. Geol.* **427**, 35–42 (2016).

38. L. F. Han, L. N. Plummer, A review of single-sample-based models and other approaches for radiocarbon dating of dissolved inorganic carbon in groundwater. *Earth Sci. Rev.* **152**, 119–142 (2016).

39. L.-F. Han, L. N. Plummer, P. Aggarwal, A graphical method to evaluate predominant geochemical processes occurring in groundwater systems for radiocarbon dating. *Chem. Geol.* **318–319**, 88–112 (2012).

40. H. H. Loosli, A dating method with ^{39}Ar. *Earth Planet. Sci. Lett.* **63**, 51–62 (1983).

41. A. Bollhöfer, C. Schlosser, S. Schmid, M. Konrad, R. Purtschert, R. Krais, Half a century of Krypton-85 activity concentration measured in air over Central Europe: Trends and relevance for dating young groundwater. *J. Environ. Radioact.* **205–206**, 7–16 (2019).

42. A. Visser, H. P. Broers, R. Purtschert, J. Sültenfuß, M. de Jonge, Groundwater age distributions at a public drinking water supply well field derived from multiple age tracers (^{85}Kr, ^{3}H/^{3}He, and ^{39}Ar). *Water Resour. Res.* **49**, 7778–7796 (2013).

43. J. A. Corcho Alvarado *et al.*, Constraining the age distribution of highly mixed groundwater using ^{39}Ar: A multiple environmental tracer (^{3}H/^{3}He, ^{85}Kr, ^{39}Ar, and ^{14}C) study in the semiconfined Fontainebleau Sands Aquifer (France). *Water Resour. Res.* **43**, W03427 (2007).

44. J. C. Vogel, Investigation of groundwater flow with radiocarbon, in *Symposium on Isototopes Hydrology* (IAEA, Vienna, 1967).

45. B. C. Jurgens, J. K. Bohlke, S. M. Eberts, *An Excel(R) Workbook for Interpreting Groundwater Age Distributions from Environmental Tracer Data* (U.S. Geological Survey, 2012); www.usgs.gov/pubprod.

46. B. R. Scanlon, I. Jolly, M. Sophocleous, L. Zhang, Global impacts of conversions from natural to agricultural ecosystems on water resources: Quantity versus quality. *Water Resour. Res.* **43**, W03437 (2007).

47. M. J. Currell, D. Han, Z. Chen, I. Cartwright, Sustainability of groundwater usage in northern China: Dependence on palaeowaters and effects on water quality, quantity and ecosystem health. *Hydrol. Process.* **26**, 4050–4066 (2012).

48. K. M. Ransom, A. M. Bell, Q. E. Barber, G. Kourakos, T. Harter, A Bayesian approach to infer nitrogen loading rates from crop and land-use types surrounding private wells in the Central Valley, California. *Hydrol. Earth Syst. Sci.* **22**, 2739–2758 (2018).

49. K. M. Lockhart, A. M. King, T. Harter, Identifying sources of groundwater nitrate contamination in a large alluvial groundwater basin with highly diversified intensive agricultural production. *J. Contam. Hydrol.* **151**, 140–154 (2013).

50. R. O. Miller, J. Kotuby-Amacher, N. Dellavalle, C. Bethel, B. Vaughan, *ASA-CSSA-SSSA International Annual Meetings (November 6–10, 2005)* (Salt Lake City, Utah, USA, 2005); https://a-c-s.confex.com/a-c-s/2005am/techprogram/P9137.HTM.

51. M. R. Nunes, J. E. Denardin, C. M. P. Vaz, D. L. Karlen, C. A. Cambardella, Lime movement through highly weathered soil profiles. *Environ. Res. Commun.* **1**, 115002 (2019).

52. E. Thomsen, R. Andreasen, Agricultural lime disturbs natural strontium isotope variations: Implications for provenance and migration studies. *Sci. Adv.* **5**, eaav8083 (2019).

53. B. K. Esser, H. Beller, C. Carlie, B. Cey, G. B. Hudson, R. Leif, T. Letain, c. Moody-Bartel, K. Moore, W. McNab, J. Moran, A. Tompson, *Nitrate Biogeochemistry and Reactive Transport in California Groundwater: LDRD Final Report* (Livermor, California, 2006).

54. J. F. Saraceno, J. T. Kulongoski, T. M. Mathany, A novel high-frequency groundwater quality monitoring system. *Environ. Monit. Assess.* **190**, 477 (2018).

55. T. L. Arnold, L. A. DeSimone, L. M. Bexfield, B. C. Lindsey, J. R. Barlow, J. T. Kulongoski, M. Musgrove, J. A. Kingsbury, K. Belitz, *Groundwater Quality Data From the National Water-Quality Assessment Project, May 2012 Through December 2013* (U.S. Geological Survey Data Series 997, 2016), p. 56.

56. M. L. Roberts, J. R. Burton, K. L. Elder, B. E. Longworth, C. P. McIntyre, K. F. . Reden, B. X. Han, B. E. Rosenheim, W. J. Jenkins, E. Galutschek, A. P. McNichol, A High-Performance14C accelerator mass spectrometry system. *Radiocarbon* **52**, 228–235 (2010).

57. M. J. Fishman, *Methods of Analysis by the U.S. Geological Survey National Water Quality Laboratory; Determination of Inorganic and Organic Constituents in Water and Fluvial Sediments* (U.S. Geological Survey Open-File Report, 93-125, 1993), p. 217.

58. J. R. Garbarino, L. K. Kanagy, M. E. Cree, *Determination of Elements in Natural-Water, Biota, Sediment, and Soil Samples Using Collision/Reaction Cell Inductively Coupled Plasma-Mass Spectrometry* (U.S. Geological Survey, 2006).

59. K. Revesz, B. Buck, T. B. Coplen, *Determination of the δ(2H/1H) and δ(18O/16O)of Soil Water and Plant Matter: RSIL Lab Code1700* (U.S. Geological Survey, 2009).

60. H. G. Oestlund, H. G. Dorsey, *Rapid Electrolytic Enrichment and Hydrogen Gas Proportional Counting of Tritium* (International conference on low radioactivity measurement and applications, 1977).

61. A. G. Hunt, *U.S. Geological Survey Noble Gas Laboratory's Standard Operating Procedures for the Measurement of Dissolved Gas in Water Samples* (U.S. Geological Survey, Reston, VA, 2015).

62. E. Mace, C. Aalseth, J. Brandenberger, A. Day, E. Hoppe, P. Humble, M. Keillor, J. Kulongoski, C. Overman, M. Panisko, A. Seifert, S. White, E. Wilcox Freeburg, R. Williams, Methods for using argon-39 to age-date groundwater using ultra-low-background proportional counting. *Appl. Radiat. Isot.* **126**, 9–12 (2017).

63. A. Visser, J. E. Moran, M. J. Singleton, B. K. Esser, Importance of river water recharge to the San Joaquin Valley groundwater system. *Hydrol. Process.* **32**, 1202–1213 (2018).

64. A. M. Seltzer, J. Ng, W. R. Danskin, J. T. Kulongoski, R. S. Gannon, M. Stute, J. P. Severinghaus, Deglacial water-table decline in Southern California recorded by noble gas isotopes. *Nat. Commun.* **10**, 5739 (2019).

65. R. F. Weiss, Carbon dioxide in water and seawater: The solubility of a non-ideal gas. *Mar. Chem.* **2**, 203–215 (1974).

66. K. Emrich, D. H. Ehhalt, J. C. Vogel, Carbon isotope fractionation during the precipitation of calcium carbonate. *Earth Planet. Sci. Lett.* **8**, 363–371 (1970).

67. J. C. Vogel, P. M. Grootes, W. G. Mook, Isotopic fractionation between gaseous and dissolved carbon dioxide. *Zeitschrift für Phys.* **230**, 225–238 (1970).

68. W. G. Mook, J. C. Bommerson, W. H. Staverman, Carbon isotope fractionation between dissolved bicarbonate and gaseous carbon dioxide. *Earth Planet. Sci. Lett.* **22**, 169–176 (1974).

69. P. Bénézeth, G. D. Saldi, J. L. Dandurand, J. Schott, Experimental determination of the solubility product of magnesite at 50 to 200°C. *Chem. Geol.* **286**, 21–31 (2011).

70. D. C. Jones, T. Ito, Y. Takano, W.-C. Hsu, Spatial and seasonal variability of the air-sea equilibration timescale of carbon dioxide. *Global Biogeochem. Cycles* **28**, 1163–1178 (2014).